

Free Vibration Analysis of a Circular Plate With Multiple Circular Holes by Using Indirect BIEM and Addition Theorem

W. M. Lee

Department of Mechanical Engineering,
China University of Science and Technology,
Taipei, Taiwan
e-mail: wmllee@cc.chit.edu.tw

J. T. Chen¹

Department of Harbor and River Engineering,
National Taiwan Ocean University,
Keelung, Taiwan
e-mail: jtchen@mail.ntou.edu.tw

In this paper, natural frequencies and natural modes of a circular plate with multiple circular holes are theoretically derived and numerically determined by using the indirect boundary integral formulation, the addition theorem, and the complex Fourier series. Owing to the addition theorem, all kernel functions are expanded into degenerate forms and further expressed in the same polar coordinate centered at one circle where the boundary conditions are specified. Avoiding not only the computation of the principal value but also the calculation of higher-order derivatives can be easily determined. By matching boundary conditions, a coupled infinite system of linear algebraic equations is derived as an analytical model for the free vibration of a circular plate with multiple circular holes. The direct-searching approach is utilized in the truncated finite system to determine the natural frequency through singular value decomposition. After determining the unknown Fourier coefficients, the corresponding mode shapes are obtained by using the indirect boundary integral formulations. Some numerical eigensolutions are presented and then utilized to explain some physical phenomenon such as the beating and the dynamic stress concentration. Good accuracy and fast rate of convergence are the main features of the present method, thanks to the analytical approach.

[DOI: 10.1115/1.4001993]

1 Introduction

Circular plates with multiple circular holes are commonly observed in engineering structures [1], e.g., aviation, aerospace, and shipping, either to reduce the weight of the whole structure, to increase the range of inspection, or to satisfy some other engineering designs. In addition, the title problem includes annularlike plates, which are common elements in the rotating machinery with practical applications including disk brake system, circular saw blades, and hard disk for data storage [2]. Geometric discontinuities due to these holes inevitably cause the change in dynamic characteristics as well as the decrease in load carrying capacity. It is important to comprehend the associated effects in the work of the mechanical design or the associated controller design. As quoted by Leissa and Narita [3], "the free vibrations of circular plates have been of practical and academic interest for at least a century and a half." We revisit this problem by proposing a semi-analytical approach.

Over the past few decades, most of the researches have focused on the analytical solutions for natural frequencies of the circular or annular plates [4–7]. Recently, some researchers intended to extend an annular plate [8,9] to the plate with an eccentric hole. Cheng et al. [8] encountered difficulty and resorted to the finite element method (FEM) to implement the vibration analysis of annularlike plates due to the complicated expression for this kind of plate. Laura et al. [9] determined the natural frequencies of a circular plate with an eccentric hole by using the Rayleigh–Ritz variational method where the assumed function does not satisfy the natural boundary condition in the inner free edge. Lee et al. [10] proposed a semi-analytical approach to solve the free vibra-

tion analysis of a circular plate with multiple holes by using the indirect boundary integral equation method (BIEM).

It is well known that the boundary element method (BEM) or the BIEM can reduce the dimension of the original problem by 1, and thus the number of the introduced unknowns is much less than that of the traditional domain type methods such as finite difference method (FDM) or FEM. For BEM applications to plate problems, readers may consult with the review article [11]. By using the BIEM to analytically solve the problem of plate with multiple holes, two problems need to be solved. One is the improper integral in the boundary integral equation; the other is that the field point and the source point locate on different circular boundaries when considering the multiply connected domain problem. These problems have been treated by using the degenerate kernel and tensor transformation [10], respectively. However, tensor transformation accompanied with the higher-order derivative, such as the computation of effective shear force, increases the complexity of computation and then deteriorates the accuracy of its solution. In addition, the collocation method in Ref. [10] belongs to the point-matching approach instead of the analytical derivation. It also increases the effort of computation since boundary nodes for collocation are required to satisfy the pointwise boundary conditions.

This paper presents an analytical model for the free vibration analysis of a circular plate with multiple circular holes by using the indirect boundary integral formulation, addition theorem, and complex Fourier series. When considering a circular plate with multiple circular holes in the indirect boundary integral formulation, the transverse displacement field is represented by all adaptive coordinates centered at each center of circles. By using the addition theorem, it is transformed into the same coordinate centered at the corresponding circle, where the boundary conditions are specified. By this way, the higher derivative such as bending moments and effective shear forces can be easily determined. According to the specified boundary conditions, a coupled infinite system of simultaneous linear algebraic equations is obtained.

¹Corresponding author.

Contributed by the Applied Mechanics of ASME for publication in the JOURNAL OF APPLIED MECHANICS. Manuscript received April 28, 2009; final manuscript received March 13, 2010; accepted manuscript posted June 16, 2010; published online XXXX-XXXX-XXXX. Assoc. Editor: Subrata Mukherjee.

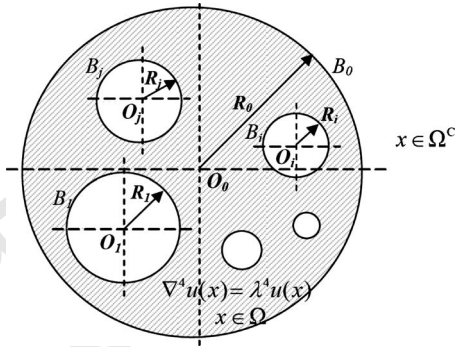


Fig. 1 Problem statement for an eigenproblem of a circular plate with multiple circular holes

Based on the direct-searching approach [12], the nontrivial eigen-
solution can be determined by finding the zero determinant of the
truncated finite system through singular value decomposition
(SVD) [13]. Several numerical examples are presented, and the
proposed results of a circular plate with an eccentric circular hole
and multiple circular holes are compared with those of semi-
analytical solutions [10], global discretization method [2], and
FEM using the ABAQUS [14]. The results of eigensolution for the
plate with two holes can be used to explain the reason why the
dynamic concentration occurs when two holes are close to each
other.

2 Problem Statement and Indirect Boundary Integral Formulation

2.1 Problem Statement of Plate Eigenproblem. A uniform
thin circular plate with H nonoverlapping circular holes centered
at the position vector O_k ($k=0, 1, \dots, H$; O_0 is the position vector
of the outer circular boundary of the plate) has a domain Ω , which
is enclosed with boundary

$$B = \bigcup_{k=0}^H B_k \quad (1)$$

as shown in Fig. 1, where R_k and B_k denote the radius and the
boundary of the k th circle, respectively. The governing equation
of the free flexural vibration for this plate is expressed as

$$\nabla^4 u(x) = \lambda^4 u(x), \quad x \in \Omega \quad (2)$$

where ∇^4 is the biharmonic operator, u is the lateral displacement,
 $\lambda^4 = \omega^2 \rho_0 h / D$, λ is the frequency parameter, ω is the circular fre-
quency, ρ_0 is the volume density, h is the plate thickness, D
 $= Eh^3 / 12(1 - \mu^2)$ is the flexural rigidity of the plate, E denotes the
Young's modulus, and μ is the Poisson's ratio

2.2 Indirect Boundary Integral Formulation. Based on the
indirect boundary integral formulation, the displacement field of
plate vibration can be represented by [15]

$$u(x) = \int_B P(s, x) \phi(s) dB(s) + \int_B Q(s, x) \psi(s) dB(s), \quad x \in \Omega \quad (3)$$

where B is the boundary of the domain Ω , s and x mean the
source and field points, respectively, $\phi(s)$ and $\psi(s)$ are the un-
known fictitious density distributions on the boundary, $P(s, x)$ and
 $Q(s, x)$ are kernel functions, which can be chosen from any two of
the four kernel functions, U , Θ , M , and V , which will be elabo-
rated on later. The kernel function $U(s, x)$ is the fundamental so-
lution, which satisfies

$$\nabla^4 U(s, x) - \lambda^4 U(s, x) = \delta(s - x) \quad (4) \quad 105$$

where $\delta(s - x)$ is the Dirac-delta function. Considering the two
singular solutions ($Y_0(\lambda r)$ and $K_0(\lambda r)$, which are the zeroth order
of the second-kind Bessel and modified Bessel functions, respec-
tively) and one regular solution ($J_0(\lambda r)$ is the zeroth order of the
first-kind Bessel function) in the fundamental solution, we have
the complex-valued kernel [12],

$$U(s, x) = \frac{1}{8\lambda^2 D} \left[Y_0(\lambda r) - iJ_0(\lambda r) + \frac{2}{\pi} K_0(\lambda r) \right] \quad (5) \quad 112$$

where $r = |s - x|$ and $i^2 = -1$. The other three kernels, $\Theta(s, x)$,
 $M(s, x)$, and $V(s, x)$ can be obtained by applying the following
slope, moment, and effective shear operators defined by

$$K_\Theta = \frac{\partial(\cdot)}{\partial n} \quad (6) \quad 116$$

$$K_M = -D \left[\mu \nabla^2(\cdot) + (1 - \mu) \frac{\partial^2(\cdot)}{\partial n^2} \right] \quad (7) \quad 117$$

$$K_V = -D \left[\frac{\partial}{\partial n} \nabla^2(\cdot) + (1 - \mu) \frac{\partial}{\partial t} \left(\frac{\partial}{\partial n} \left(\frac{\partial}{\partial t}(\cdot) \right) \right) \right] \quad (8) \quad 118$$

to the kernel $U(s, x)$ with respect to the source point, where $\partial/\partial n$
and $\partial/\partial t$ are the normal and tangential derivatives, respectively;
 ∇^2 means the Laplacian operator. In the polar coordinate of (R, γ) ,
the normal and tangential derivatives can be expressed by $\partial/\partial R$
and $(1/R) \partial/\partial \gamma$, respectively, and then the three kernel functions
can be rewritten as

$$\Theta(s, x) = K_{\Theta, s}(U(s, x)) = \frac{\partial U(s, x)}{\partial R} \quad (9) \quad 125$$

$$M(s, x) = K_{M, s}(U(s, x)) = -D \left[\mu \nabla_s^2 U(s, x) + (1 - \mu) \frac{\partial^2 U(s, x)}{\partial R^2} \right] \quad (10) \quad 126$$

$$V(s, x) = K_{V, s}(U(s, x)) = -D \left[\frac{\partial}{\partial R} (\nabla_s^2 U(s, x)) + (1 - \mu) \right. \\ \left. \times \left(\frac{1}{R} \right) \frac{\partial}{\partial \gamma} \left(\frac{\partial}{\partial R} \left(\frac{1}{R} \frac{\partial U(s, x)}{\partial \gamma} \right) \right) \right] \quad (11) \quad 128$$

Since the kernels $P(s, x)$ and $Q(s, x)$ can be selected from any
two of the four kernels, $U(s, x)$, $\Theta(s, x)$, $M(s, x)$, and $V(s, x)$, six
(C_2^4) formulations can be considered. For the computational effi-
ciency, the kernels $U(s, x)$ and $\Theta(s, x)$ are chosen as $P(s, x)$ and
 $Q(s, x)$ in Eq. (3). In addition to the displacement, the slope, the
normal moment, and the effective shear force are derived by ap-
plying the three operators in Eqs. (6)–(8) to Eq. (3) with respect to
the field point as follows:

$$u(x) = \int_B U(s, x) \phi(s) dB(s) + \int_B \Theta(s, x) \psi(s) dB(s), \quad x \in \Omega \quad (12) \quad 137$$

$$\theta(x) = \int_B U_\theta(s, x) \phi(s) dB(s) + \int_B \Theta_\theta(s, x) \psi(s) dB(s), \quad x \in \Omega \quad (13) \quad 138$$

$$m(x) = \int_B U_m(s, x) \phi(s) dB(s) + \int_B \Theta_m(s, x) \psi(s) dB(s), \quad x \in \Omega \quad (14) \quad 139$$

$$v(x) = \int_B U_v(s, x) \phi(s) dB(s) + \int_B \Theta_v(s, x) \psi(s) dB(s), \quad x \in \Omega \quad (15)$$

For the clamped case, the lateral displacement $u(x)$ and the slope $\theta(x)$ on the boundary are specified to be zero. For the free case, the normal moment $m(x)$ and the effective shear force $v(x)$ on the boundary are set to be zero. The simply supported

condition can be obtained by specifying both the lateral displacement $u(x)$ and the normal moment $m(x)$ to be zero.

2.3 Degenerate Kernels and Complex Fourier Series for the Fictitious Boundary Densities. In the polar coordinates, the field point and source point can be expressed as $x=(\rho, \phi)$ and $s=(R, \gamma)$, respectively. By using the addition theorem [16], the kernel functions $U(s, x)$ and $\Theta(s, x)$ are expanded in the series form as follows:

$$U: \begin{cases} U^I(s, x) = \frac{1}{8\lambda^2 D} \sum_{m=-\infty}^{\infty} \left\{ J_m(\lambda \rho) [Y_m(\lambda R) - iJ_m(\lambda R)] + \frac{2}{\pi} I_m(\lambda \rho) K_m(\lambda R) \right\} e^{im(\phi-\gamma)}, & \rho < R \\ U^E(s, x) = \frac{1}{8\lambda^2 D} \sum_{m=-\infty}^{\infty} \left\{ J_m(\lambda R) [Y_m(\lambda \rho) - iJ_m(\lambda \rho)] + \frac{2}{\pi} I_m(\lambda R) K_m(\lambda \rho) \right\} e^{im(\phi-\gamma)}, & \rho \geq R \end{cases} \quad (16)$$

$$\Theta: \begin{cases} \Theta^I(s, x) = \frac{1}{8\lambda D} \sum_{m=-\infty}^{\infty} \left\{ J_m(\lambda \rho) [Y'_m(\lambda R) - iJ'_m(\lambda R)] + \frac{2}{\pi} I_m(\lambda \rho) K'_m(\lambda R) \right\} e^{im(\phi-\gamma)}, & \rho < R \\ \Theta^E(s, x) = \frac{1}{8\lambda D} \sum_{m=-\infty}^{\infty} \left\{ J'_m(\lambda R) [Y_m(\lambda \rho) - iJ_m(\lambda \rho)] + \frac{2}{\pi} I'_m(\lambda R) K_m(\lambda \rho) \right\} e^{im(\phi-\gamma)}, & \rho \geq R \end{cases} \quad (17)$$

where the superscripts I and E denote the interior and exterior cases for $U(s, x)$ degenerate kernel to distinguish $\rho < R$ and $\rho > R$, respectively, as shown in Fig. 2. The other degenerate kernels $U_\theta(s, x)$, $\Theta_\theta(s, x)$, $U_m(s, x)$, $\Theta_m(s, x)$, $U_v(s, x)$, and $\Theta_v(s, x)$ in the indirect boundary integral equations can be obtained by applying the operators of Eqs. (6)–(8) to the degenerate kernel $U(s, x)$ and $\Theta(s, x)$ in Eqs. (16) and (17) with respect to the field point x . In order to fully utilize the geometry of circular boundary, the fictitious boundary densities, $\phi(s)$ and $\psi(s)$, can be expanded by employing the complex Fourier series as follows:

$$\phi^k(s) = \sum_{n=-\infty}^{\infty} a_n^k e^{in\gamma_k}, \quad s \in B_k, \quad k=0, \dots, H \quad (18)$$

$$\psi^k(s) = \sum_{n=-\infty}^{\infty} b_n^k e^{in\gamma_k}, \quad s \in B_k, \quad k=0, \dots, H \quad (19)$$

where a_n^k and b_n^k are the complex Fourier coefficients of the k th circular boundary, γ_k is its polar angle and H is the number of inner holes.

3 Eigensolutions for a Circular Plate With Multiple Circular Holes

Considering a circular plate with H circular holes, Eq. (12) can be explicitly expressed as

$$u(x) = \int_{B_0} U^I(s_0, x) \phi(s_0) dB_0(s_0) + \int_{B_0} \Theta^I(s_0, x) \psi(s_0) dB_0(s_0) - \left[\sum_{k=1}^H \int_{B_k} U^E(s_k, x) \phi(s_k) dB_k(s_k) + \int_{B_k} \Theta^E(s_k, x) \psi(s_k) dB_k(s_k) \right], \quad x \in \Omega \quad (20)$$

Substituting both the degenerate kernels, Eqs. (16) and (17), and the fictitious boundary densities, Eqs. (18) and (19), into Eq. (20) in the adaptive coordinate system yields

$$u(x; \rho_0, \phi_0, \rho_1, \phi_1, \dots, \rho_H, \phi_H) = \int_{B_0} \left(\frac{1}{8\lambda^2 D} \sum_{m=-\infty}^{\infty} \left\{ J_m(\lambda \rho_0) [Y_m(\lambda R_0) - iJ_m(\lambda R_0)] + \frac{2}{\pi} I_m(\lambda \rho_0) K_m(\lambda R_0) \right\} e^{im(\phi_0-\gamma_0)} \right) \left(\sum_{n=-\infty}^{\infty} a_n^0 e^{in\gamma_0} \right) dB_0(s_0) + \int_{B_0} \left(\frac{1}{8\lambda D} \sum_{m=-\infty}^{\infty} \left\{ J'_m(\lambda \rho_0) [Y'_m(\lambda R_0) - iJ'_m(\lambda R_0)] + \frac{2}{\pi} I'_m(\lambda \rho_0) K'_m(\lambda R_0) \right\} e^{im(\phi_0-\gamma_0)} \right) \left(\sum_{n=-\infty}^{\infty} b_n^0 e^{in\gamma_0} \right) dB_0(s_0)$$

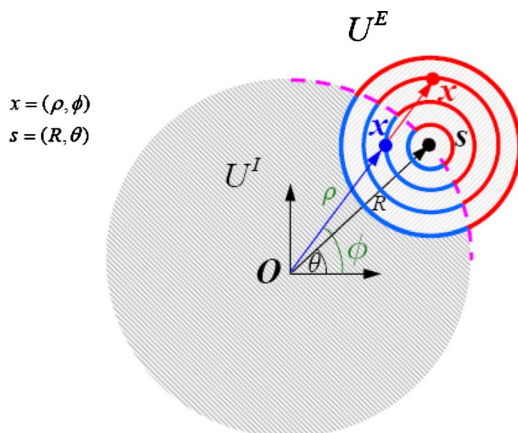


Fig. 2 Degenerate kernel for $U(s, x)$

$$\begin{aligned}
 & - \sum_{k=1}^H \left[\int_{B_k} \left(\frac{1}{8\lambda^2 D} \sum_{m=-\infty}^{\infty} \left\{ J_m(\lambda R_k) [Y_m(\lambda \rho_k) - iJ_m(\lambda \rho_k)] \right. \right. \right. \\
 & \left. \left. \left. + \frac{2}{\pi} I_m(\lambda R_k) K_m(\lambda \rho_k) \right\} e^{im(\phi_k - \gamma_k)} \right) \left(\sum_{n=-\infty}^{\infty} a_n^k e^{in\gamma_k} \right) dB_k(s_k) \right. \\
 & \left. + \int_{B_k} \frac{1}{8\lambda D} \sum_{m=-\infty}^{\infty} \left\{ J'_m(\lambda R_k) [Y_m(\lambda \rho_k) - iJ_m(\lambda \rho_k)] \right. \right. \\
 & \left. \left. + \frac{2}{\pi} I'_m(\lambda R_k) K_m(\lambda \rho_k) \right\} e^{im(\phi_k - \gamma_k)} \left(\sum_{n=-\infty}^{\infty} b_n^k e^{in\gamma_k} \right) dB_k(s_k) \right]
 \end{aligned} \quad (21)$$

where the $(\rho_0, \phi_0), (\rho_1, \phi_1), \dots, (\rho_H, \phi_H)$ are the coordinates of the field point x in the local coordinates at the center of the corresponding circle. By employing the analytical integration along each circular boundary in the adaptive coordinate and by applying the orthogonal property, Eq. (21) can be rewritten as

$$\begin{aligned}
 & u(x; \rho_0, \phi_0, \rho_1, \phi_1, \dots, \rho_H, \phi_H) \\
 & = \frac{\pi R_0}{4\lambda^2 D} \sum_{m=-\infty}^{\infty} \left\{ J_m(\lambda \rho_0) [Y_m(\lambda R_0) - iJ_m(\lambda R_0)] \right. \\
 & \left. + \frac{2}{\pi} I_m(\lambda \rho_0) K_m(\lambda R_0) \right\} a_m^0 e^{im\phi_0} + \frac{\pi R_0}{4\lambda D} \sum_{m=-\infty}^{\infty} \left\{ J_m(\lambda \rho_0) [Y'_m(\lambda R_0) \right. \\
 & \left. - iJ'_m(\lambda R_0)] + \frac{2}{\pi} I_m(\lambda \rho_0) K'_m(\lambda R_0) \right\} b_m^0 e^{im\phi_0} \\
 & - \sum_{k=1}^H \left[\frac{\pi R_k}{4\lambda^2 D} \sum_{m=-\infty}^{\infty} \left\{ J_m(\lambda R_k) [Y_m(\lambda \rho_k) - iJ_m(\lambda \rho_k)] \right. \right. \\
 & \left. \left. + \frac{2}{\pi} I_m(\lambda R_k) K_m(\lambda \rho_k) \right\} a_m^k e^{im\phi_k} + \frac{\pi R_k}{4\lambda D} \sum_{m=-\infty}^{\infty} \left\{ J'_m(\lambda R_k) [Y_m(\lambda \rho_k) \right. \right. \\
 & \left. \left. - iJ'_m(\lambda \rho_k)] + \frac{2}{\pi} I'_m(\lambda R_k) K_m(\lambda \rho_k) \right\} b_m^k e^{im\phi_k} \right]
 \end{aligned} \quad (22)$$

To determine these unknown coefficients, the other three Eqs. (13)–(15) are required by applying three operators of Eqs. (9)–(11) to Eq. (22). First, this procedure involves the higher-order derivatives. Second, Eq. (22) consists of several different variables. It is difficult to directly derive the formulation. Consequently, it is necessary to transform Eq. (22) into one coordinate system by applying again the addition theorem.

Based on the Graf's addition theorem for the Bessel functions given in Refs. [16,17], we can express the theorem in the following form:

$$J_m(\lambda \rho_k) e^{im\phi_k} = \sum_{n=-\infty}^{\infty} J_{m-n}(\lambda r_{kp}) e^{i(m-n)\theta_{kp}} J_n(\lambda \rho_p) e^{in\phi_p} \quad (23)$$

$$I_m(\lambda \rho_k) e^{im\phi_k} = \sum_{n=-\infty}^{\infty} I_{m-n}(\lambda r_{kp}) e^{i(m-n)\theta_{kp}} I_n(\lambda \rho_p) e^{in\phi_p} \quad (24)$$

$$\begin{aligned}
 & Y_m(\lambda \rho_k) e^{im\phi_k} \\
 & = \begin{cases} \sum_{n=-\infty}^{\infty} Y_{m-n}(\lambda r_{kp}) e^{i(m-n)\theta_{kp}} J_n(\lambda \rho_p) e^{in\phi_p}, & \rho_p < r_{kp} \\ \sum_{n=-\infty}^{\infty} J_{m-n}(\lambda r_{kp}) e^{i(m-n)\theta_{kp}} Y_n(\lambda \rho_p) e^{in\phi_p}, & \rho_p > r_{kp} \end{cases}
 \end{aligned} \quad (25)$$

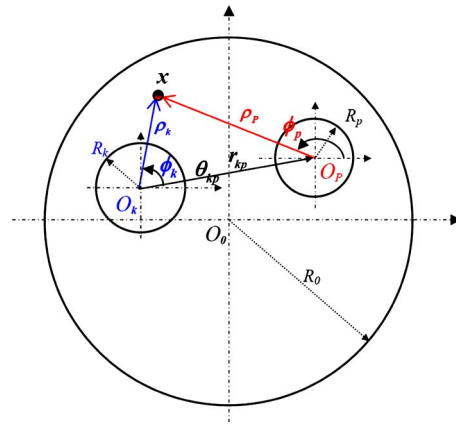


Fig. 3 Notation of Graf's addition theorem for Bessel functions

$$\begin{aligned}
 & K_m(\lambda \rho_k) e^{im\phi_k} \\
 & = \begin{cases} \sum_{n=-\infty}^{\infty} (-1)^n K_{m-n}(\lambda r_{kp}) e^{i(m-n)\theta_{kp}} I_n(\lambda \rho_p) e^{in\phi_p}, & \rho_p < r_{kp} \\ \sum_{n=-\infty}^{\infty} (-1)^{m-n} I_{m-n}(\lambda r_{kp}) e^{i(m-n)\theta_{kp}} K_n(\lambda \rho_p) e^{in\phi_p}, & \rho_p > r_{kp} \end{cases}
 \end{aligned} \quad (26)$$

where (ρ_p, ϕ_p) and (ρ_k, ϕ_k) in Fig. 3 are the polar coordinates of a general field point x with respect to O_p and O_k , which are the origins of two polar coordinate systems, and (r_{kp}, θ_{kp}) are the polar coordinates of O_k with respect to O_p .

By using the addition theorem for the Bessel functions $J_m(\lambda \rho_k)$, $Y_m(\lambda \rho_k)$, and $K_m(\lambda \rho_k)$, the displacement field near the circular boundary B_0 under the condition of $\rho_0 > r_{k0}$ can be expanded as follows:

$$\begin{aligned}
 & u(x; \rho_0, \phi_0) \\
 & = \frac{\pi R_0}{4\lambda^2 D} \sum_{m=-\infty}^{\infty} \left\{ J_m(\lambda \rho_0) [Y_m(\lambda R_0) - iJ_m(\lambda R_0)] \right. \\
 & \left. + \frac{2}{\pi} I_m(\lambda \rho_0) K_m(\lambda R_0) \right\} a_m^0 e^{im\phi_0} \\
 & + \frac{\pi R_0}{4\lambda D} \sum_{m=-\infty}^{\infty} \left\{ J_m(\lambda \rho_0) [Y'_m(\lambda R_0) - iJ'_m(\lambda R_0)] \right. \\
 & \left. + \frac{2}{\pi} I_m(\lambda \rho_0) K'_m(\lambda R_0) \right\} b_m^0 e^{im\phi_0} \\
 & - \sum_{k=1}^H \left[\frac{\pi R_k}{4\lambda^2 D} \sum_{m=-\infty}^{\infty} \left\{ J_m(\lambda R_k) \sum_{n=-\infty}^{\infty} J_{m-n}(\lambda r_{k0}) e^{i(m-n)\theta_{k0}} [Y_n(\lambda \rho_0) \right. \right. \\
 & \left. \left. - iJ_n(\lambda \rho_0)] \right. \right. \\
 & \left. + \frac{2}{\pi} I_m(\lambda R_k) \sum_{n=-\infty}^{\infty} (-1)^{m-n} I_{m-n}(\lambda r_{k0}) e^{i(m-n)\theta_{k0}} K_n(\lambda \rho_0) \right\} e^{in\phi_0} a_m^k \\
 & + \frac{\pi R_k}{4\lambda D} \sum_{m=-\infty}^{\infty} \left\{ J'_m(\lambda R_k) \sum_{n=-\infty}^{\infty} J_{m-n}(\lambda r_{k0}) e^{i(m-n)\theta_{k0}} [Y_n(\lambda \rho_0) \right. \\
 & \left. - iJ_n(\lambda \rho_0)] \right. \\
 & \left. + \frac{2}{\pi} I'_m(\lambda R_k) \sum_{n=-\infty}^{\infty} (-1)^{m-n} I_{m-n}(\lambda r_{k0}) \right.
 \end{aligned}$$

$$\times e^{i(m-n)\theta_{k0}} K_n(\lambda \rho_0) \left\{ e^{in\phi_0} b_m^k \right\} \quad (27)$$

Furthermore, Eq. (27) can be rewritten as

$$u(x; \rho_0, \phi_0) = \sum_{m=-\infty}^{\infty} e^{im\phi_0} \left\{ A_m^0(\lambda \rho_0) a_m^0 + B_m^0(\lambda \rho_0) b_m^0 \right. \\ \left. - \sum_{k=1}^H \left[\sum_{n=-\infty}^{\infty} A_{mn}^k(\lambda \rho_0) a_n^k + \sum_{n=-\infty}^{\infty} B_{mn}^k(\lambda \rho_0) b_n^k \right] \right\} \quad (28)$$

where

$$A_m^0(\lambda \rho_0) = \frac{\pi R_0}{4\lambda^2 D} \left\{ J_m(\lambda \rho_0) [Y_m(\lambda R_0) - iJ_m(\lambda R_0)] \right. \\ \left. + \frac{2}{\pi} I_m(\lambda \rho_0) K_m(\lambda R_0) \right\} \quad (29)$$

$$B_m^0(\lambda \rho_0) = \frac{\pi R_0}{4\lambda D} \left\{ J_m(\lambda \rho_0) [Y'_m(\lambda R_0) - iJ'_m(\lambda R_0)] \right. \\ \left. + \frac{2}{\pi} I_m(\lambda \rho_0) K'_m(\lambda R_0) \right\} \quad (30)$$

$$A_{mn}^0(\lambda \rho_0) = \frac{\pi R_k}{4\lambda^2 D} e^{i(n-m)\theta_{k0}} \left\{ J_{n-m}(\lambda r_{k0}) J_n(\lambda R_k) [Y_m(\lambda \rho_0) \right. \\ \left. - iJ_m(\lambda \rho_0)] + \frac{2}{\pi} (-1)^{n-m} I_{n-m}(\lambda r_{k0}) I_n(\lambda R_k) K_m(\lambda \rho_0) \right\} \quad (31)$$

$$B_{mn}^0(\lambda \rho_0) = \frac{\pi R_k}{4\lambda D} e^{i(n-m)\theta_{k0}} \left\{ J_{n-m}(\lambda r_{k0}) J'_n(\lambda R_k) [Y_m(\lambda \rho_0) - iJ_m(\lambda \rho_0)] \right. \\ \left. + \frac{2}{\pi} (-1)^{n-m} I_{n-m}(\lambda r_{k0}) I'_n(\lambda R_k) K_m(\lambda \rho_0) \right\} \quad (32)$$

By differentiating Eq. (28) with respect to ρ_0 , the slope θ near the circular boundary B_0 is given as

$$E_{mn}^k(\lambda \rho_p) = \begin{cases} \frac{\pi R_k}{4\lambda^2} e^{i(n-m)\theta_{kp}} \left\{ J_{n-m}(\lambda r_{kp}) \alpha_m^J(\lambda \rho_p) [Y_n(\lambda R_k) - iJ_n(\lambda R_k)] + \frac{2}{\pi} J_{n-m}(\lambda r_{kp}) \alpha_m^I(\lambda \rho_p) K_n(\lambda R_k) \right\}, & k=0 \\ \frac{\pi R_k}{4\lambda^2} e^{i(n-m)\theta_{kp}} \left\{ \alpha_m^J(\lambda \rho_p) J_n(\lambda R_k) [Y_{n-m}(\lambda r_{kp}) - iJ_{n-m}(\lambda r_{kp})] + \frac{2}{\pi} (-1)^m \alpha_m^I(\lambda \rho_p) I_n(\lambda R_k) K_{n-m}(\lambda r_{kp}) \right\}, & k \neq 0, p \end{cases} \quad (37)$$

$$F_{mn}^k(\lambda \rho_p) = \begin{cases} \frac{\pi R_k}{4\lambda} e^{i(n-m)\theta_{kp}} \left\{ J_{n-m}(\lambda r_{kp}) \alpha_m^J(\lambda \rho_p) [Y'_n(\lambda R_k) - iJ'_n(\lambda R_k)] + \frac{2}{\pi} J_{n-m}(\lambda r_{kp}) \alpha_m^I(\lambda \rho_p) K'_n(\lambda R_k) \right\}, & k=0 \\ \frac{\pi R_k}{4\lambda} e^{i(n-m)\theta_{kp}} \left\{ \alpha_m^J(\lambda \rho_p) J'_n(\lambda R_k) [Y_{n-m}(\lambda r_{kp}) - iJ_{n-m}(\lambda r_{kp})] + \frac{2}{\pi} (-1)^m \alpha_m^I(\lambda \rho_p) I'_n(\lambda R_k) K_{n-m}(\lambda r_{kp}) \right\}, & k \neq 0, p \end{cases} \quad (38)$$

where the moment operator $\alpha_m^X(\lambda \rho)$ from Eq. (7) is defined as

$$\alpha_m^X(\lambda \rho) = D \left\{ (1-\mu) \frac{X'_m(\lambda \rho)}{\rho} - \left[(1-\mu) \frac{m^2}{\rho^2} \mp \lambda^2 \right] X_m(\lambda \rho) \right\} \quad (39)$$

in which the upper (lower) signs refer to $X=J, Y$ (I, K), respectively. The differential equations for the Bessel's functions have been used to simplify $\alpha_m^X(\lambda \rho)$.

$$\theta(x; \rho_0, \phi_0) = \sum_{m=-M}^M e^{im\phi_0} \left\{ C_m^0(\lambda \rho_0) a_m^0 + D_m^0(\lambda \rho_0) b_m^0 \right. \\ \left. - \sum_{k=1}^H \left[\sum_{n=-\infty}^{\infty} C_{mn}^k(\lambda \rho_0) a_n^k + \sum_{n=-\infty}^{\infty} D_{mn}^k(\lambda \rho_0) b_n^k \right] \right\} \quad (33)$$

where $C_m^0(\lambda \rho_0)$, $D_m^0(\lambda \rho_0)$, $C_{mn}^k(\lambda \rho_0)$, and $D_{mn}^k(\lambda \rho_0)$ can be obtained by differentiating $A_m^0(\lambda \rho_0)$, $B_m^0(\lambda \rho_0)$, $A_{mn}^k(\lambda \rho_0)$, and $B_{mn}^k(\lambda \rho_0)$ in Eqs. (29)–(32) with respect to ρ_0 .

Similarly, by applying the addition theorem to Eq. (22) and then using the moment operator of Eq. (7), the bending moment field $m(x)$ near the circular boundary B_p ($p=1, \dots, H$) can be expanded as follows:

$$m(x; \rho_p, \phi_p) = \sum_{m=-\infty}^{\infty} e^{im\phi_p} \left\{ E_m^p(\lambda \rho_p) a_m^p + F_m^p(\lambda \rho_p) b_m^p \right. \\ \left. - \sum_{k=0}^H \varepsilon_k \left[\sum_{n=-\infty}^{\infty} E_{mn}^k(\lambda \rho_p) a_n^k + \sum_{n=-\infty}^{\infty} F_{mn}^k(\lambda \rho_p) b_n^k \right] \right\} \quad (34)$$

where $\varepsilon_k = -1$, $k=0$, and $\varepsilon_k = 1$, $k \neq 0$,

$$E_m^p(\lambda \rho_p) = \frac{\pi R_p}{4\lambda^2} \left\{ J_m(\lambda R_p) [\alpha_m^Y(\lambda \rho_p) - i\alpha_m^J(\lambda \rho_p)] \right. \\ \left. + \frac{2}{\pi} I_m(\lambda R_p) \alpha_m^K(\lambda \rho_p) \right\} \quad (35)$$

$$F_m^p(\lambda \rho_p) = \frac{\pi R_p}{4\lambda} \left\{ J'_m(\lambda R_p) [\alpha_m^Y(\lambda \rho_p) - i\alpha_m^J(\lambda \rho_p)] \right. \\ \left. + \frac{2}{\pi} I'_m(\lambda R_p) \alpha_m^K(\lambda \rho_p) \right\} \quad (36)$$

From Eq. (8), the effective shear operator $\beta_m^X(\lambda \rho)$ can be expressed as follows:

$$\beta_m^X(\lambda \rho) = D \left\{ [m^2(1-\mu) \pm (\lambda \rho)^2] \frac{X'_m(\lambda \rho)}{\rho^2} - m^2(1-\mu) \frac{X_m(\lambda \rho)}{\rho^3} \right\} \quad (40)$$

287 Similarly, the effective shear field $v(x)$ near the circular bound-
288 ary B_p ($p=1, \dots, H$) can be expressed as follows:

$$289 \quad v(x; p_p, \phi_p) = \sum_{m=-\infty}^{\infty} e^{im\phi_p} \left[G_m^p(\lambda \rho_p) a_m^p + H_m^p(\lambda \rho_p) b_m^p \right. \\ \left. + \sum_{\substack{k=1 \\ k \neq p}}^H \varepsilon_k \left[\sum_{n=-\infty}^{\infty} G_{mn}^k(\lambda \rho_p) a_n^k + \sum_{n=-\infty}^{\infty} H_{mn}^k(\lambda \rho_p) b_n^k \right] \right] \quad (41)$$

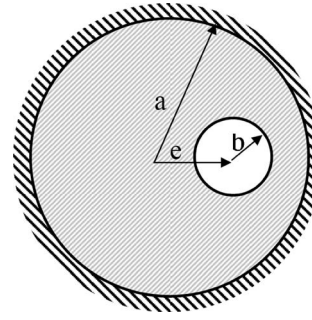
291 where $G_m^p(\lambda \rho_p)$, $H_m^p(\lambda \rho_p)$, $G_{mn}^k(\lambda \rho_p)$, and $H_{mn}^k(\lambda \rho_p)$ are obtained
292 by replacing $\alpha_m^X(\lambda \rho_p)$ in Eqs. (35)–(38) by $\beta_m^X(\lambda \rho_p)$.

293 For an outer clamped circular plate ($u=\theta=0$) with multiple cir-
294 cular holes subject to free edge ($m=v=0$), by setting ρ_p to R_p and
295 applying the orthogonal property of $\{e^{im\phi_p}\}$ ($p=0, 1, \dots, H$), Eqs.
296 (28), (33), (34), and (41) yield

$$297 \quad A_m^0(\lambda R_0) a_m^0 + B_m^0(\lambda R_0) b_m^0 - \sum_{k=1}^H \left[\sum_{n=-\infty}^{\infty} A_{mn}^k(\lambda R_0) a_n^k \right. \\ \left. + \sum_{n=-\infty}^{\infty} B_{mn}^k(\lambda R_0) b_n^k \right] = 0 \\ 298 \\ 299 \quad C_m^0(\lambda R_0) a_m^0 + D_m^0(\lambda R_0) b_m^0 - \sum_{k=1}^H \left[\sum_{n=-\infty}^{\infty} C_{mn}^k(\lambda R_0) a_n^k \right. \\ \left. + \sum_{n=-\infty}^{\infty} D_{mn}^k(\lambda R_0) b_n^k \right] = 0 \\ 300 \\ 301 \quad E_m^p(\lambda R_p) a_m^p + F_m^p(\lambda R_p) b_m^p + \sum_{\substack{k=0 \\ k \neq p}}^H \varepsilon_k \left[\sum_{n=-\infty}^{\infty} E_{mn}^k(\lambda R_p) a_n^k \right. \\ \left. + \sum_{n=-\infty}^{\infty} F_{mn}^k(\lambda R_p) b_n^k \right] = 0 \\ 302 \\ 303 \quad G_m^p(\lambda R_p) a_m^p + H_m^p(\lambda R_p) b_m^p + \sum_{\substack{k=0 \\ k \neq p}}^H \varepsilon_k \left[\sum_{n=-\infty}^{\infty} G_{mn}^k(\lambda R_p) a_n^k \right. \\ \left. + \sum_{n=-\infty}^{\infty} H_{mn}^k(\lambda R_p) b_n^k \right] = 0 \\ 304 \\ 305$$

306 for $m=0, \pm 1, \pm 2, \dots$, $n=0, \pm 1, \pm 2, \dots$, and $p=1, \dots, H$. Equa-
307 tion (42) results in a coupled infinite system of simultaneous lin-
308 ear algebraic equations for the coefficients a_m^k and b_m^k , k
309 $=0, \dots, H$.

310 For an outer free circular plate ($m=v=0$) with multiple circular
311 holes subject to a clamped edge ($u=\theta=0$), a coupled infinite sys-
312 tem of linear equations analogous to Eq. (42) can be similarly
313 obtained as follows: (1) $A_m^0(\lambda R_0)$, $B_m^0(\lambda R_0)$, $A_{mn}^k(\lambda R_0)$, and
314 $B_{mn}^k(\lambda R_0)$ in Eq. (42) are determined by replacing $X_m(\lambda \rho_0)$ in Eqs.
315 (29)–(32) with $\alpha_m^X(\lambda \rho_0)$ and setting ρ_0 to R_0 , where the notation X
316 represents J , Y , I , and K , respectively; (2) $C_m^0(\lambda R_0)$, $D_m^0(\lambda R_0)$,
317 $C_{mn}^k(\lambda R_0)$, and $D_{mn}^k(\lambda R_0)$ in Eq. (42) can be similarly obtained,
318 but here $\beta_m^X(\lambda \rho_p)$ is used; (3) $E_m^p(\lambda R_p)$, $F_m^p(\lambda R_p)$, $E_{mn}^k(\lambda R_p)$, and
319 $F_{mn}^k(\lambda R_p)$ in Eq. (42) are determined by replacing $\alpha_m^X(\lambda \rho_0)$ in Eqs.
320 (35)–(38) with $X_m(\lambda \rho_0)$ and setting ρ_0 to R_0 ; and (4) differentiat-
321 ing the coefficients in (3) with respect to ρ_0 and setting ρ_0 to R_0
322 yield $G_m^p(\lambda R_p)$, $H_m^p(\lambda R_p)$, $G_{mn}^k(\lambda R_p)$, and $H_{mn}^k(\lambda R_p)$ in Eq. (42).



Case 1:

Geometric data:
 $a=1\text{m}$
 $b=0.25\text{m}$
 $e=0.45\text{m}$
thickness=0.002m
Boundary condition:
Inner circle : free
Outer circle: clamped

Fig. 4 A circular plate with an eccentric hole subject to clamped-free boundary conditions

In the following computation, only the finite M terms are used 323
in Eq. (42). Based on the direct-searching scheme [12], the natural 324
frequencies are determined as the minimum singular value from 325
the SVD of the truncated finite system by performing the fre- 326
quency sweep. In our approach, two steps are employed. In the 327
first step, the larger frequency interval $\Delta\lambda$ is taken. For example, 328

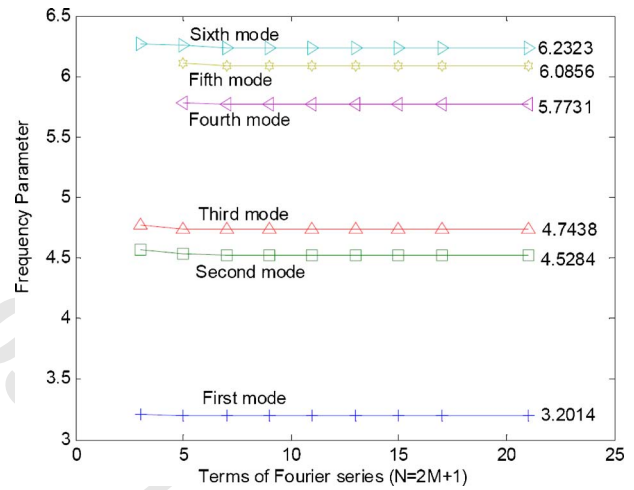


Fig. 5 Natural frequency parameter versus the number of terms of Fourier series for a circular plate with an eccentric hole ($a=1.0$, $b=0.25$, $e/a=0.45$)

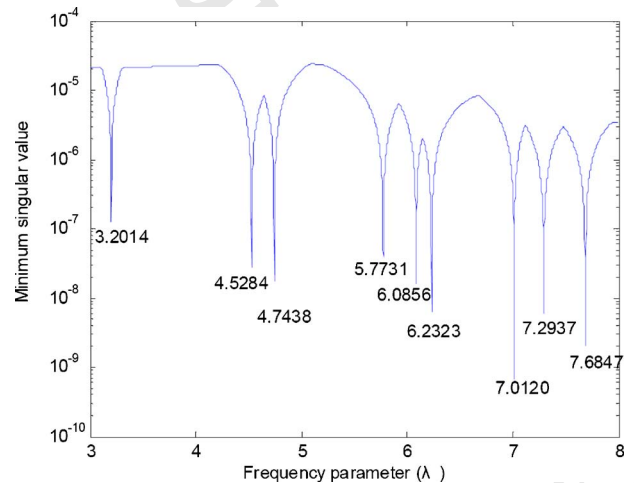


Fig. 6 The minimum singular value versus the frequency parameter for a circular plate with one eccentric hole ($a=1.0$, $b=0.25$, $e=0.45$)

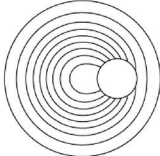
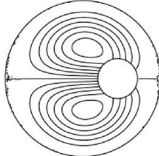
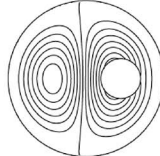
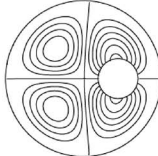
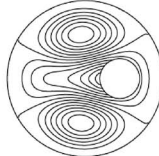
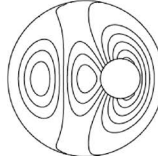
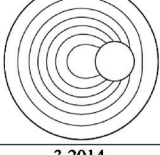
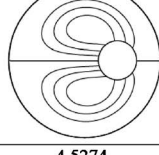
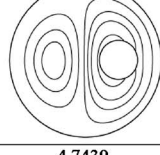
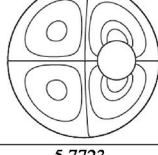
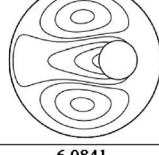
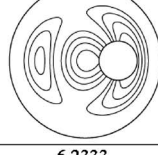
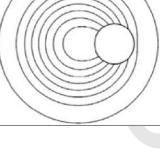
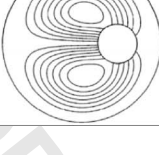
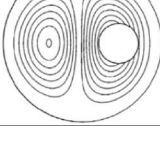
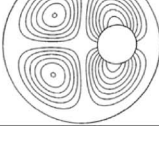
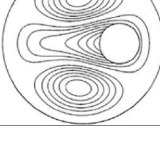
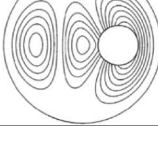
Mode No.	1	2	3	4	5	6
Approach	3.2014	4.5284	4.7438	5.7731	6.0856	6.2323
Present method						
Approach	3.1870	4.5210	4.7400	5.7580	6.0600	6.2560
Semi-analytical method [10]						
Approach	3.2014	4.5274	4.7439	5.7723	6.0841	6.2333
ABAQUS						

Fig. 7 The lower six natural frequency parameters and modes of a circular plate with an eccentric hole ($a=1.0$, $b=0.25$, $e=0.45$)

the value of 0.1 is chosen to sweep the frequency range of our concern. For the second step, the local sweep with the smaller one proceeded depending on the precision requirement of the considered problem. For instance, the value of 0.0001 is adopted in this paper. That is to say, the adaptive scheme of $\Delta\lambda$ is used. Once the eigenvalues are found, the associated mode shapes can be obtained by substituting the corresponding boundary eigenvectors (i.e., the complex Fourier series representing the fictitious boundary density) into the boundary integral equations.

4 Numerical Results and Discussions

To demonstrate the proposed method, the FORTRAN code was implemented to determine natural frequencies and modes of a circular plate with multiple circular holes. The same problem was independently solved by using FEM (the ABAQUS software) for comparison. In all cases, the inner boundary is subject to the free boundary condition, the thickness of the plate is 0.002 m, and the Poisson's ratio μ is 1/3 unless otherwise specified. The general-purpose linear triangular elements of type S3 were employed to model the plate problem by using ABAQUS. Although the thickness of the plate is 0.002 m, these elements do not suffer from the transverse shear locking based on the theoretical manual of ABAQUS [14].

4.1 Case 1: A Circular Plate With an Eccentric Hole [2,10]. A circular plate with an eccentric hole, as shown in Fig. 4, is considered. The outer and inner radii are 1 m ($R_1=1$ m) and 0.25 m ($R_2=0.25$ m), respectively, and the offset distance e for the eccentric hole is 0.45 m ($e/a=0.45$). The lower six natural frequency parameters versus the number of terms of Fourier series N are shown in Fig. 5. It shows that the proposed solution promptly converges by using only a few terms of Fourier series. In addition, only the fourth and fifth modes are lost in the former six modes when M equals to 1. The convergence rate is superior to that by using the collocation approach [10] for the same problem. Figure 6 indicates the minimum singular value of the influence matrix versus the frequency parameter λ when using 11 terms of Fourier series ($N=11$). Since the direct-searching scheme is used, the drop location indicates the eigenvalue. The FEM was employed to solve the same problem, and its model has 242,211 elements and 121,891 nodes in order to obtain acceptable results for comparison. The lower six natural frequency parameters and

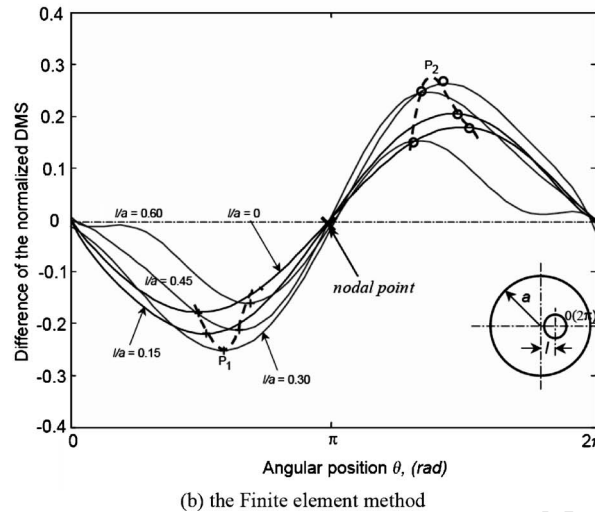
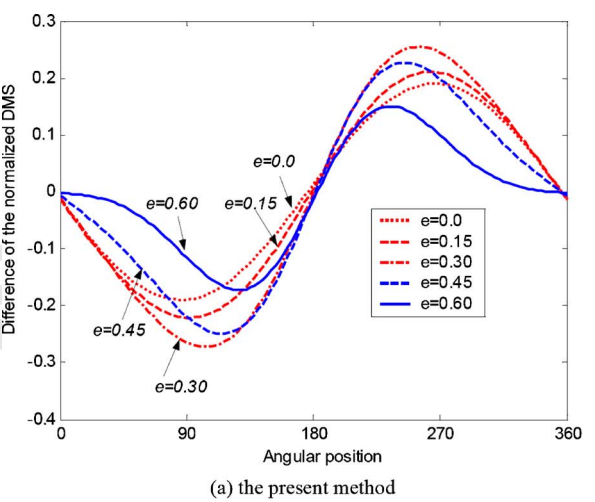


Fig. 8 Contour of residual DMSs around the hole with eccentricity e from 0 to 0.6: (a) the present method and (b) the finite element method [8]

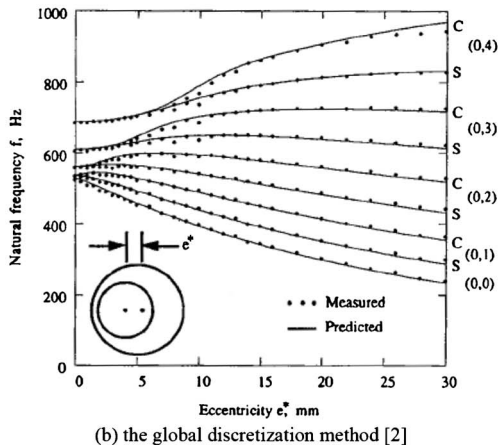
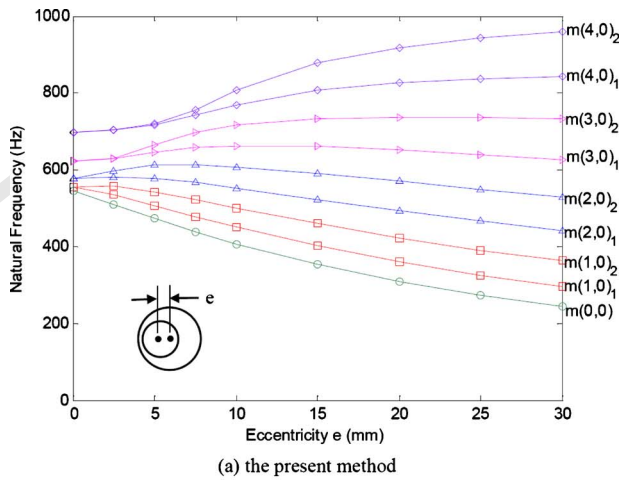


Fig. 9 Effect of the eccentricity e on the natural frequencies for the free-clamped annularlike plate: (a) the present method and (b) the global discretization method [2]

369 modes by using the present method, the semi-analytical method
370 [10], and FEM are shown in Fig. 7. The results of the present
371 method match well with those of FEM by using ABAQUS. It indi-
372 cates that the semi-analytical results show some deviations from
373 the other results due to the complicated transformation of the ef-
374 fective shear force.

375 It may be worth mentioning that the proposed method can per-
376 form a local vibration analysis by using the residual displacement
377 mode shape (DMS), defined as the difference of DMS between the
378 circular and annularlike plate to the problem of damage detection
379 [8]. Figure 8 shows the contour of residual DMSs of mode (1,0)
380 [10] around the hole with eccentricity e from 0 to 0.6 by using (a)

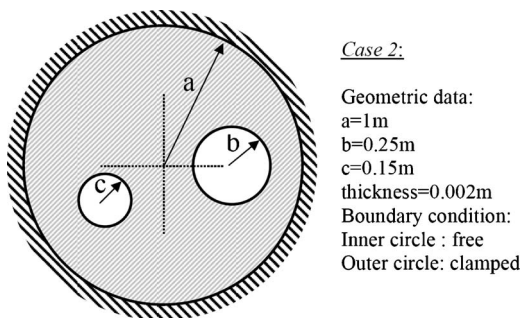


Fig. 10 A circular plate with two holes subject to clamped-free boundary conditions

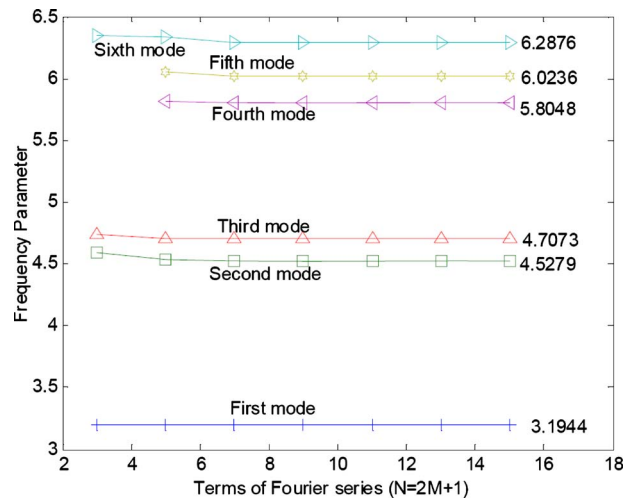


Fig. 11 Natural frequency parameter versus the number of terms of Fourier series for a circular plate with two holes ($a=1.0$, $b=0.25$, $c=0.15$)

the present method and (b) the finite element method [8]. The
unobvious change around the hole in the DMS, even for a small
eccentricity, can be detected clearly from the residual DMS analy-
sis. It can provide an approach to identify damage occurring in the
annularlike plate.

The next example is a commercial computer hard disk drive
[2], which is an annular aluminum plate. The outer and inner radii
are 178 mm and 84 mm, respectively, and the thickness is 1.9 mm.
The plate was fixtured between two solid circular aluminum
flanges with an outside radius of 124 mm. The flanges were
aligned and positioned on the plate at a specified value of e within
the range of 0–30 mm. Figure 9 is the effect of the eccentricity e
on the natural frequencies for the free-clamped annularlike plate
by using (a) the present method and (b) the global discretization
method. Good agreement can be observed. Values of m and n in
the mode (m,n) [10] shown in Fig. 9 are numbers of diametrical
nodal lines and circular nodal lines, respectively. Subscript 1 de-
notes the straight diametrical nodal line, while subscript 2 denotes
the curved diametrical nodal line [10]. It shows that an annularlike
plate with small eccentricity has close eigenfrequencies and is apt
to result in beating between those close eigenmodes.

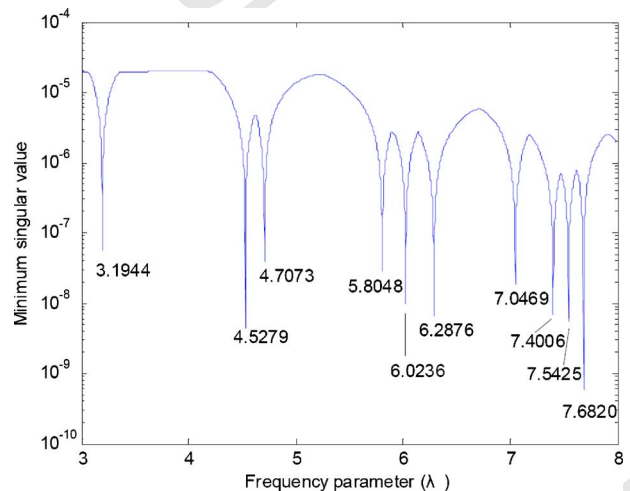


Fig. 12 The minimum singular value versus the frequency parameter for a circular plate with two holes ($a=1.0$, $b=0.25$, $c=0.15$)

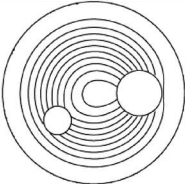
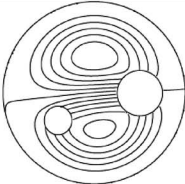
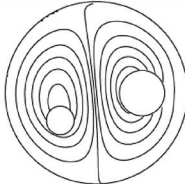
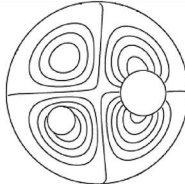
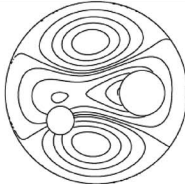
Mode No.	1	2	3	4	5
Approach	3.1944	4.5279	4.7073	5.8048	6.0236
Present method					
Semi-analytical method [9]	3.1770	4.5290	4.699	5.7510	5.9570
ABAQUS	3.1943	4.5270	4.7089	5.8062	6.0222

Fig. 13 The lower five natural frequency parameters and modes of a circular plate with two holes ($a=1.0$, $b=0.25$, $c=0.15$)

4.2 Case 2: A Circular Plate With Two Holes [10]. In order to demonstrate the generality of the present method, a circular plate with two holes is considered, as shown in Fig. 10. The radii of holes are 0.25 m and 0.15 m, and the coordinates of the centers are (0.5, 0.0) and (−0.4, −0.3), respectively. The lower six natural frequency parameters versus the number of terms of Fourier series N are shown in Fig. 11. When the number of inner circular hole increases, the fast convergence rate can also be observed. The sixth mode shows a slower convergence rate due to the complex geometrical configuration. Figure 12 indicates the minimum singular value of the influence matrix versus the frequency parameter λ when using 11 terms of Fourier series ($N=11$). To achieve a comparable solution for comparison, the FEM needs 136,670 elements. The lower five natural frequency parameters and modes by using the present method, the semi-analytical method [10], and FEM are shown in Fig. 13. Good agreement between the results of the present method and those of ABAQUS is observed.

To investigate the hole-hole interaction [18], a circular plate containing two identical holes with different central distances is studied. The radii of the circular plate and the circular hole are 1 m and 0.15 m, and the dimensionless distances of two holes L/a are chosen as 2.1, 2.5, and 4.0 in the numerical experiments, where a is the radius of circular holes and L is the central distance of two holes. Numerical results show that the space of two holes has a minor effect on the lower eigenfrequencies. Regarding eigenmodes shown in Fig. 14, the zone of the maximum deformation, enclosed with the dashed line, for the case of $L/a=2.1$ is significantly less than that for $L/a=4.0$. Consequently, the dynamic stress concentration [19] for the case of $L/a=2.1$ is larger because the distortion energy caused by the external loading concentrates in the smaller area.

Our proposed method has advantages over both the analytical methods and the numerical methods, such as the conventional BEM or FEM. On one hand, it is clearly convinced that the proposed formulation is applicable to problems with multiple circular holes, which cannot be solved easily by the other analytical methods. On the other hand, it is demonstrated that the proposed method has advantages, such as the good accuracy and fast rate of convergence over the conventional BEM or FEM.

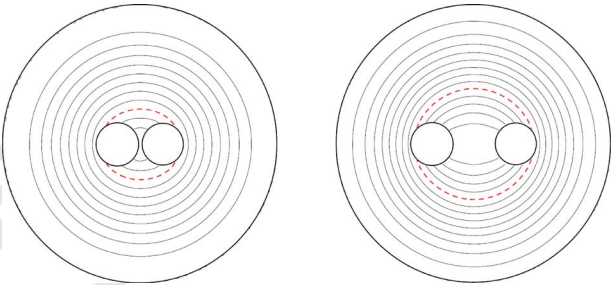


Fig. 14 The first natural frequency parameters and modes of a circular plate with two holes: (a) $L/a=2.1$ and (b) $L/a=4.0$

5 Concluding Remarks

An analytical model for the free vibration of a circular plate with multiple circular holes was derived as a coupled infinite system of simultaneous linear algebraic equations. Natural frequencies and natural modes of the stated problem were determined in the truncated finite system by using the direct-searching scheme. The proposed method utilized indirect boundary integral equations, the addition theorem, and the complex Fourier series. Owing to the addition theorem, two critical problems of improper integration in the indirect boundary integration and the higher derivative in the multiply connected domain problems were successively solved in a novel way. The proposed results match well with those provided by FEM using a lot of elements to obtain acceptable solutions for comparison. It shows good accuracy and fast rate of convergence, thanks to the analytical approach. Besides, the proposed numerical results have attempted explanations for the beating in the rotating machinery and the dynamic stress concentration when two holes are close to each other.

References

[1] Khurasia, H. B., and Rawtani, S., 1978, "Vibration Analysis of Circular Plates With Eccentric Hole," ASME J. Appl. Mech., 45, pp. 215–217.
[2] Tseng, J. G., and Wickert, J. A., 1994, "Vibration of an Eccentrically Clamped

463 Annular Plate," ASME J. Appl. Mech., **116**, pp. 155–160. 484
464 [3] Leissa, A. W., and Narita, Y., 1980, "Natural Frequencies of Simply Supported 485
465 Circular Plates," J. Sound Vib., **70**, pp. 221–229. 486
466 [4] Vogel, S. M., and Skinner, D. W., 1965, "Natural Frequencies of Transversely 487
467 Vibrating Uniform Annular Plates," ASME J. Appl. Mech., **32**, pp. 926–931. 488
468 [5] Vega, D. A., Vera, S. A., Sanchez, M. D., and Laura, P. A. A., 1998, "Trans- 489
469 verse Vibrations of Circular, Annular Plates With a Free Inner Boundary," J. 490
470 Acoust. Soc. Am., **103**, pp. 1225–1226. 491
471 [6] Vera, S. A., Sanchez, M. D., Laura, P. A. A., and Vega, D. A., 1998, "Trans- 492
472 verse Vibrations of Circular, Annular Plates With Several Combinations of 493
473 Boundary Conditions," J. Sound Vib., **213**(4), pp. 757–762. 494
474 [7] Vera, S. A., Laura, P. A. A., and Vega, D. A., 1999, "Transverse Vibrations of 495
475 a Free-Free Circular Annular Plate," J. Sound Vib., **224**(2), pp. 379–383. 496
476 [8] Cheng, L., Li, Y. Y., and Yam, L. H., 2003, "Vibration Analysis of Annular- 497
477 Like Plates," J. Sound Vib., **262**, pp. 1153–1170. 498
478 [9] Laura, P. A. A., Masia, U., and Avalos, D. R., 2006, "Small Amplitude, Trans- 499
479 verse Vibrations of Circular Plates Elastically Restrained Against Rotation 500
480 With an Eccentric Circular Perforation With a Free Edge," J. Sound Vib., **292**, 501
481 pp. 1004–1010. 502
482 [10] Lee, W. M., Chen, J. T., and Lee, Y. T., 2007, "Free Vibration Analysis of 503
483 Circular Plates With Multiple Circular Holes Using Indirect BIEMs," J. Sound 504
Vib., **304**, pp. 811–830.
[11] Providakis, C. P., and Beskos, D. E., 1999, "Dynamic Analysis of Plates by
Boundary Elements," Appl. Mech. Rev., **52**(7), pp. 213–236.
[12] Kitahara, M., 1985, *Boundary Integral Equation Methods in Eigenvalue Problems of Elastodynamics and Thin Plates*, Elsevier, Amsterdam.
[13] IMSL, 1999, *Math/Library Volumes 1 and 2*, Version 4.01, Visual Numerics, Inc.
[14] ABAQUS 6.5, 2004, Hibbitt, Karlsson and Sorensen, Inc., RI.
[15] Nagaya, K., and Poltorak, K., 1989, "Method for Solving Eigenvalue Problems of the Helmholtz Equation With a Circular Outer and a Number of Eccentric Circular Inner Boundaries," J. Acoust. Soc. Am., **85**, pp. 576–581.
[16] Watson, G. N., 1995, *A Treatise on the Theory of Bessel Functions*, 2nd ed., Cambridge Library, Cambridge.
[17] Martin, P. A., 2006, *Multiple Scattering Interaction of Time-Harmonic Wave With N Obstacles*, Cambridge University Press, Cambridge.
[18] Chandra, A., Huang, Y., Wei, X., and Hu, K. X., 1995, "A Hybrid Micro-Macro BEM Formulation for Micro-Crack Clusters in Elastic Components," Int. J. Numer. Methods Eng., **38**(7), pp. 1215–1236.
[19] Lee, W. M., and Chen, J. T., 2008, "Scattering of Flexural Wave in Thin Plate With Multiple Holes by Using the Null-Field Integral Equation Approach," Comput. Model. Eng. Sci., **1124**(1), pp. 1–30.

AUTHOR QUERIES — 022005AMJ

- #1

Au: Please supply the postal codes in the affiliation addresses.
- #2

Au: Please verify accuracy of this sentence: “Avoiding not only the computation of the principal value but also the calculation of higher-order derivatives can be easily determined.”